Applied Energy xxx (2008) xxx–xxx

Contents lists available at ScienceDirect

Applied Energy

journal homepage: www.elsevier.com/locate/apenergy

Modeling hourly and daily fractions of UV, PAR and NIR to global solar radiation under various sky conditions at Botucatu, Brazil

João F. Escobedo [a], Eduardo N. Gomes [a], Amauri P. Oliveira [b,*], Jacyra Soares [b]

[a] Department of Natural Resources, School of Agronomic Sciences, State University of São Paulo, Botucatu, São Paulo, Brazil
[b] Department of Atmospheric Sciences, Institute of Astronomy, Geophysics and Atmospheric Sciences, University of São Paulo, São Paulo, Brazil

ARTICLE INFO

Article history:
Received 13 November 2007
Received in revised form 16 April 2008
Accepted 18 April 2008
Available online xxxx

Keywords:
Global UV
PAR
NIR solar components
Global solar radiation
Clearness index
Percent UV
PAR
NIR ratios
Botucatu
Brazil

ABSTRACT

In this analysis, using available hourly and daily radiometric data performed at Botucatu, Brazil, several empirical models relating ultraviolet (UV), photosynthetically active (PAR) and near infrared (NIR) solar global components with solar global radiation (G) are established. These models are developed and discussed through clearness index K_T (ratio of the global-to-extraterrestrial solar radiation). Results obtained reveal that the proposed empirical models predict hourly and daily values accurately. Finally, the overall analysis carried out demonstrates that the sky conditions are more important in developing correlation models between the UV component and the global solar radiation. The linear regression models derived to estimate PAR and NIR components may be obtained without sky condition considerations within a maximum variation of 8%. In the case of UV, not taking into consideration the sky condition may cause a discrepancy of up to 18% for hourly values and 15% for daily values.

1. Introduction

The knowledge of ultraviolet (0.29–0.385 μm), photosynthetically active (0.385–0.7 μm) and near infrared (0.7–3.0 μm) spectral components of global solar radiation (G) at the surface becomes an imperative requirement in different technological and scientific applications of solar radiation information.

Ultraviolet radiation has been used in cleaning processes of photodecomposition of organic residues present in contaminated industrial waters [1]; photo degradation of plastics; dye, natural and synthetic fibers [2]. UV exposition is strongly correlated to cataract and skin cancer [3]. Knowing how UV component of solar radiation behaves at the surface is also important to estimate tropospheric trace gas reactions in polluted areas [4] and to reduce the uncertainty in the in- and out-door chamber reactions of atmospheric pollutants [5].

The resultant effects of sky conditions, water vapour, aerosol load and ozone amount on the UV radiant flux has been extensively investigated through ground observations [6–22] that in turn reveal that the linear correlation between UV versus global solar radiation (G). Ground UV and G measurements grouping into hourly, daily monthly and annual data sets revealed that the fraction of UV radiant flux to global solar radiation ranges between 2% and 9.4% over several localities worldwide.

The smallest values of UV fractions can be attributed to the scattering effect aerosol and gases presents in the atmosphere. According to the Rayleigh theory, the intensity of scattered energy is directly proportional to the inverse fourth power of the wavelength. Therefore, UV is more affected by scattering than G. Besides, absorption of UV by particulate matter produced by dust, air pollution events and episodic tropospheric ozone high concentrations in urban areas may also further deplete more UV than G. Indeed, observations indicated that atmospheric dust always reduces more UV than G. Elhadidy et al. [7] reported UV/G values ranging from 2.1% to 4.5% in Dhahran (Saudi Arabia); Khogali and Al-Bar [8] found values ranging from 2.8% to 4.3% in Makkah (Saudi Arabia); Robaa [9] reported fractions ranging from 2.2% to 2.7% for polluted air and between 3.2% and 3.5% for unpolluted areas of Cairo (Egypt). The observations carried out in Kuwait by Al-Aruri et al. [10] yields UV/G ranging from 4.3% to 5.2%. In this case, there is no apparent reason for the high UV/G values in Kuwait since dust is the major source of particulate matter and the climate is very similar (low relative humidity and predominance of cloudless days) to the previously mentioned studies.

* Corresponding author. Tel.: +55 11 3091 4701; fax: +55 11 3091 4714.
E-mail address: apdolive@usp.br (A.P. Oliveira).

0306-2619/$ - see front matter © 2008 Elsevier Ltd. All rights reserved.
doi:10.1016/j.apenergy.2008.04.013

Nomenclature

G	global solar radiation
UV	ultraviolet solar radiation
PAR	photosynthetically active solar radiation
NIR	near infrared solar radiation
I_G	global solar irradiance at the surface (W m^{-2})
I_{UV}	ultraviolet solar irradiance at the surface solar at the surface (W m^{-2})
I_{PAR}	photosynthetically active solar irradiance at the surface (W m^{-2})
I_{NIR}	near infrared solar irradiance at the surface (W m^{-2})
K_T	clearness index
K_T^h	hourly value of clearness index
K_T^d	daily value of clearness index
H_G^h	hourly value of global solar irradiance at the surface (MJ m^{-2})
H_{UV}^h	hourly value of UV component of solar irradiance at the surface (MJ m^{-2})
H_{PAR}^h	hourly value of PAR component of solar irradiance at the surface (MJ m^{-2})
H_{NIR}^h	hourly value of NIR component of solar irradiance at the surface (MJ m^{-2})
H_G^d	daily value of global solar irradiance at the surface (MJ m^{-2})
H_{UV}^d	daily value of UV component of solar irradiance at the surface (MJ m^{-2})
H_{PAR}^d	daily value of PAR component of solar irradiance at the surface (MJ m^{-2})
H_{NIR}^d	daily value of NIR component of solar irradiance at the surface (MJ m^{-2})
b_{UV}^h	slope of the best-fit straight line for hourly UV data
b_{PAR}^h	slope of the best-fit straight line for hourly PAR data
b_{NIR}^h	slope of the best-fit straight line for hourly NIR data
b_{UV}^d	slope of the best-fit straight line for daily UV data
b_{PAR}^d	slope of the best-fit straight line for daily PAR data
b_{NIR}^d	slope of the best-fit straight line for daily NIR data
MBE	mean bias error
RMSE	root mean square error
d	index of agreement
R^2	coefficient of determination
G_{top}	extraterrestrial solar radiation
I_0	solar flux at the top of the atmosphere
D	actual Sun–Earth distance
$\overline{D}$	average distance between the Sun and the Earth
S_0	average solar constant
Z	solar zenith angle
b_{sky}	slope of the best-fit straight line considering sky conditions
$b_{without}$	slope of the best-fit straight line without sky condition consideration

On the other hand, the largest values of UV/G occur in the presence of clouds. The main reason for this is that clouds are associated with high contents of water vapour in the atmosphere that, in turn absorbs more G than UV increasing UV/G. For instance, it was observed in Kwangju, South Korea, UV/G fractions between 7.0% and 9.4%, reflecting the large content of water vapour of the Kwanju (Ogunjobi and Kim [11]). Comparatively, the UV/G fractions found in the Mediterranean region by Cañada et al. [12] and Foyo-Moreno et al. [13] are smaller. The UV/G fraction values observed in Spanish cities – between 4.4% and 5.6% (Valencia), 3.9% and 4.4% (Córdoba) and 3.0% to 5.0% (Granada) – were closed linked to the relative humidity variations.

Photosynthetically active radiation plays an essential role in the photosynthesis, being fundamental for physiological processes in the agronomic and forest areas, related mainly to the characterization and morphology of plants [23], estimating of plant interaction and competition [24] and documenting temporal variations in the canopy structure [25] and in the assessment of crop productivity.

In the case of the PAR component, most of these works indicated that the presence of cloud increases PAR fraction of the global radiation (PAR/G) [26–43]. As in UV band, higher fraction (PAR/G) values are likely to be associated with water vapour absorption process that in turn alters significantly more the global solar radiation leaving unaltered the PAR portion of the spectrum. Scattering caused by aerosol is a secondary effect in PAR [44].

Despite the important interaction with water vapour, near infrared solar radiation at the surface is less investigated compared with UV and PAR. The NIR properties at the top of the atmosphere are well known due to the application in remote sensing technique to retrieve the total column water vapour amount [45]. The NIR radiation represents a large amount of the total energy of the solar spectrum, around 46.5% in Brazil [46] and 51.8% in Tibet Plateau [47].

The near infrared radiation is strongly absorbed by water vapour and its interaction with cloud is not very well documented observationally [48]. Most of the work related to the NIR is based on modeling [49,50].

The objective of this work is to develop and validate empirical expressions to estimate hourly and daily values of UV, PAR and NIR in terms of G measured at surface considering only the effect of clouds. This could be particularly relevant in tropical and subtropical regions, like Brazil, where cloud plays an important role in the climate.

Here, cloud effect on solar radiation will be taking into consideration assuming sky conditions objectively specified in terms of four intervals of clearness index (K_T): (i) cloudy ($K_T \leqslant 0.35$); (*ii*) partially cloudy with predominance of diffuse component of the solar radiation ($0.35 < K_T \leqslant 0.55$); (*iii*) partially cloudy with predominance of direct component of the solar radiation ($0.55 < K_T \leqslant 0.65$) and (*iv*) clear sky ($K_T \leqslant 0.65$).

The methodology developed here to classify sky condition – based on the use of simultaneous measurements of global, diffuse and direct solar radiation – is a new method that combines all the available methodology and yields a classification procedure more objective than the other methods available in the literature. For instance, Iqbal [51] used the clearness index to classify the sky condition; Rao [6] categorized the sky in terms of fractional sunshine, whereas Perez et al. [52], Alados et al. [36] and Jacovides et al. [42,43], employed the sky clearness and brightness.

A second novelty in this work is that for the first time 5-year long series of simultaneous measurement of G, UV and NIR is used to determine UV, PAR and NIR fractions of global solar radiation and to develop regression models considering the four sky classification mentioned above.

2. Site and measurements

The data used in this work was measured at the radiometric station, at 22°53′S of latitude and 48°26′W of longitude, located in the rural area of Botucatu city, in the country side of State of São Paulo, Brazil (Fig. 1a). Botucatu, a city with 119.3 thousand habitants, is located in the countryside of Brazil, at 786 m above the mean sea level, and approximately 221 km far from the Atlantic Ocean (Fig.

Please cite this article in press as: Escobedo JF et al., Modeling hourly and daily fractions of UV, PAR and NIR to global solar ..., Appl Energ (2008), doi:10.1016/j.apenergy.2008.04.013

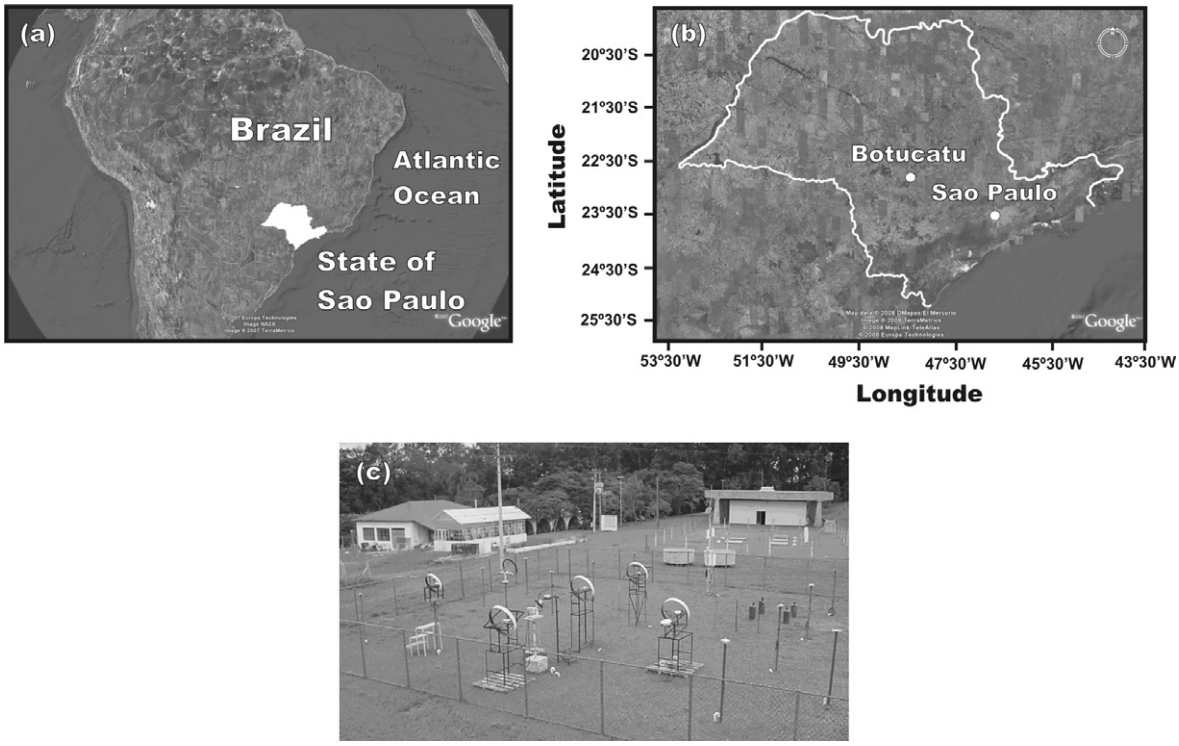

Fig. 1. Geographic position of the (a) State of São Paulo; (b) Botucatu and (c) view of the NW quadrant of the Radiometric Station in Botucatu, State of São Paulo, Brazil.

1b). It is characterized by mild cold and dry winter (June–August) and by warm and wet summer (December–February). The averaged air temperature varies from a minimum of 16.5 °C in the winter to a maximum of 23.9 °C in the summer. The minimum precipitation occurs in August and the maximum in January [53].

The radiometric station of Botucatu (Fig. 1c) belongs to the School of Agronomic Sciences, State University of São Paulo, and it has been monitoring since 2001, continuously and simultaneously global solar radiation, ultraviolet solar radiation and near infrared solar radiation at the surface.

The global solar irradiance (I_G) was measured by an Eppley pyranometer, model *PSP* (0.3–3 μm). The ultraviolet portion of solar irradiance (I_{UV}) was measured by Kipp-Zonen pyranometer, model CUV-*3* (0.29–0.39 μm). The near infrared portion of solar irradiance (I_{NIR}) was measured by an Eppley pyranometer, model *PSP*, with a filter that allows transmission of solar radiation only between 0.7 and 3.0m. Following the manufacture recommendation the calibration factor used in the filtered pyranometer was multiplied by 0.92 to correct effects of filter transmission on the sensor. Calibration of solar radiation sensors were performed every two years using procedure recommended by OMM [54].

Photosynthetically active radiation (I_{PAR}) values used in this analysis were determined indirectly through the following equation: $I_{PAR} = I_G - (I_{UV} + I_{NIR})$ Here, the PAR unit is the same as the UV, NIR and G, in W m^{-2} for irradiance, and in MJ m^{-2} for daily and hourly irradiances. Most published PAR values are expressed in photo-biological units (μE m^{-2} or μmol m^{-2} s) giving the number of photons that fall in the spectral interval 0.4–0.7 μm. To comparing PAR values obtained here against those reported in the literature, when necessary, McCree's [55] conversion factor of 4.57 μE J^{-1} was used.

From 2001 to 2005, three pyranometers were operating continuously using a data acquisition system Datalogger Campbell, model *CR23X*. The measurements were sampled with frequency of 1 Hz and 5-min averaged values were performed of all three irradiances.

Data was inspected and suspicious values were removed from the series. Due to the sensor or the data acquisition system malfunctions, it was removed 1 day in 2001, 15 days in 2002, 6 days in 2003, 80 days in 2004 and 37 days in 2005. Observations carried out between 0530 local time (LT) and 0730 LT and between 1730 LT and 1930 LT were also removed from the data set due to blocking effects caused by obstacles near to the horizon (Fig. 1c). It was removed 1431 h of observations carried out in 2001, 1441 h in 2002, 1420 h in 2003, 1771 h in 2004 and 1459 h in 2005.

Hourly and daily values of solar radiant fluxes used in this analysis are indicated as H_x^y; here, subscript implies respective spectral solar component, whereas superscript gives integrated time interval. For example, H_G^h, H_{UV}^h, H_{PAR}^h and H_{NIR}^h denote hourly values and H_G^d, H_{UV}^d, H_{PAR}^d and H_{NIR}^d denote daily values of solar radiant fluxes, respectively.

Hourly and daily values were estimated for the entire period of 5 years (2001–2005). To develop the empirical expressions to estimate UV, PAR and NIR components of solar radiation it was used data from 2001 to 2004. Validation of all expressions was carried out using data from 2005.

The extraterrestrial solar radiation used in the evaluation of the clearness index was estimated by $G_{top} = -I_0 \cos Z$, with I_0 being the solar flux at the top of the atmosphere given by $I_0 = (\bar{D}/D)^2 S_0$, where $\bar{D}$ is the average distance between the Sun and the Earth, D is the actual Sun–Earth distance, S_0 is the average solar constant assumed equal to 1366 W m^{-2} [56] and Z is the solar zenith angle calculated according to Iqbal [51].

3. Results and discussion

3.1. Sky condition classification

Prior to the analysis of the correlation results between the spectral UV, PAR and NIR bands and the global solar radiation, it is constructive to categorize the sky conditions at the Botucatu site. For

Please cite this article in press as: Escobedo JF et al., Modeling hourly and daily fractions of UV, PAR and NIR to global solar ..., Appl Energ (2008), doi:10.1016/j.apenergy.2008.04.013

that purpose, as in [57–58], the hourly clearness index K_T^h is evaluated, based on the continuous observations (1995–2003) of global, diffuse [59] and direct solar beam components. Keeping in mind the above, four sky categories have been considered here:

Interval i: $K_T^h \leqslant 0.35$ and direct component of the global solar radiation at the surface is practically zero. Therefore, global and diffuse solar radiations are equal and the sky condition is defined as totally covered cloud or cloudy sky;

Interval ii: $0.35 < K_T^h \leqslant 0.55$. The global solar radiation at the surface is composed by a fraction of diffuse component that is larger than the fraction of direct component, and the diffuse fraction is decreasing with K_T^h. The upper limit of this interval is set where diffuse equals direct component of the solar radiation (approximately at 200 W m^{-2} and at $K_T^h = 0.55$). In this case, the sky condition is defined as partially cloudy with predominance of diffuse component of the solar radiation because the radiation field is predominantly composed by diffuse radiation;

Interval iii: $0.55 < K_T \geqslant 0.65$. The global solar radiation at the surface is composed by a fraction of diffuse component that is smaller than the fraction of direct component and the diffuse fraction is decreasing with K_T until 0.65, considered as the end of the partially cloudy interval [51]. In this case, the sky condition is partially cloudy with predominance of direct component of the solar radiation because the direct beam predominantly composes the radiation field;

Interval iv: $K_T^h > 0.65$. The global solar radiation at the surface is composite by direct component of solar radiation and the diffuse contribution is very small, indicating that there is no significant cloud cover. In this case the sky condition is clear sky.

Fig. 2 indicates the block-averaged curves for global, direct and diffuse solar radiation in terms of K_T^h. These curves were obtained by dividing the variation interval of K_T^h (0–1) into 100 sub-intervals and block-averaging values of global, direct and diffuse solar radiations for each sub-interval of $K_{T_i}^h$. The choice of the subinterval size of 0.01 was obtained by trail-and-error, compromising the smoothest curve and the statistical significance associated to the number of values in each sample for all three solar radiation components.

Considering the frequency distribution diagram of hourly values of K_T^h (Fig. 3a), from 12,569 hourly values of G, about 2566 values were located within *i* interval, 2525 values within *ii* interval;

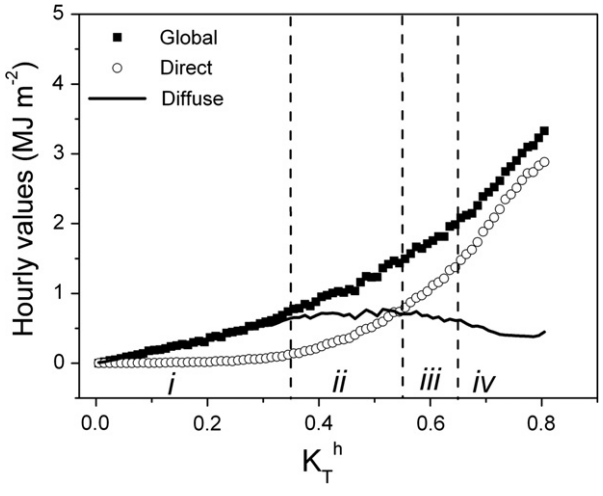

Fig. 2. Block-average values of global, diffuse and direct components of solar radiation, at the surface, in terms of clearness index intervals. Vertical dashed lines define regions of K_T values associated to sky condition and identified by *i* (cloudy sky), *ii* (partially cloudy with predominance of diffuse component of the solar radiation), *iii* (partially cloudy with predominance of direct component of the solar radiation) and *iv* (clear sky). Based on hourly values observed continuously in Botucatu from 1995 to 2003.

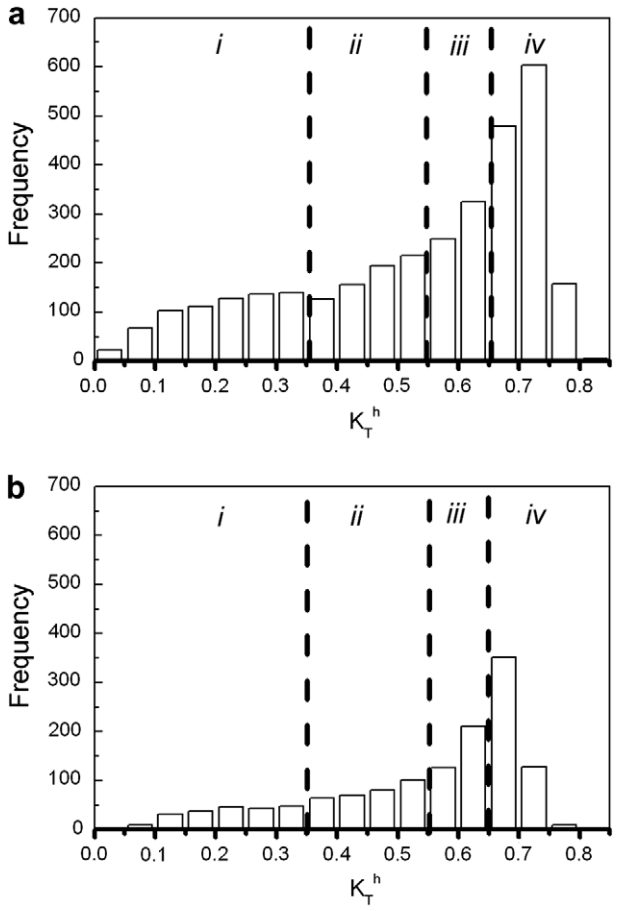

Fig. 3. Frequency distribution of (a) hourly and (b) daily values of clearness index for Botucatu. It was considered 1359 days (12,565 h) of observations between January 1, 2001 and December 31, 2004. Vertical dashed lines define regions of K_T values associated to the sky conditions.

2128 within *iii* interval and 5350 values within *iv* interval. Similarly, the frequency distribution diagram of daily values of K_T^d (Fig. 3b) from a total of 1359 days shows that 217 days is within *i* interval; 215 days in *ii* interval; 271 days in *iii* interval and 490 days in *iv* interval.

The models developed in this work are based on the correlation between hourly and daily values of H_{UV}, H_{PAR} and H_{NIR} and hourly and daily values of H_G. They were developed by linear regression, passing through the origin, considering the sky condition given by the different intervals of K_T .

Tables 1 and 2 indicate the statistical properties of UV, PAR and NIR considering hourly and daily values, respectively, for the four sky conditions given by the four intervals of K_T. There, the number of hours and days refers to the total period of time when simultaneous measurements of global solar radiation and its three components were available in Botucatu. For reference, it was included in Tables 1 and 2 the linear expressions and determination coefficients for hourly and daily values estimated not considering sky conditions. These expressions are valid for Botucatu for $0 \leqslant K_T \leqslant 1$. All the statistics shown here were performed using data from 2001 to 2004.

3.2. Hourly values

In general, the hourly fractions of UV and PAR components to global solar radiation, namely (UV/G) and (PAR/G), increase as sky conditions changed from clear to overcast; by contrast, the

Table 1
Statistical properties of hourly values of G, UV, PAR and NIR considering the four sky conditions in terms of hourly values of clearness index

Clearness index interval	Radiation component	Fraction of G (%)	Maximum (MJ m^{-2})	Number of hours
$K_r^h \leqslant 0.35$	G	–	1.92	2566
	UV	5.03	0.09	2566
	PAR	51.74	1.03	2566
	NIR	43.23	0.81	2566
$0.35 < K_T^h \leqslant 0.55$	G	–	2.76	2525
	UV	4.43	0.13	2525
	PAR	49.29	1.57	2525
	NIR	46.28	1.29	2525
$0.55 < K_T^h \leqslant 0.65$	G	–	3.27	2128
	UV	4.11	0.15	2128
	PAR	48.82	1.78	2128
	IV	47.07	1.53	2128
$K_T^h > 0.65$	G	–	4.14	5350
	UV	4.04	0.18	5350
	PAR	49.00	2.18	5350
	NIR	46.96	1.97	5350
$0 \leqslant K_T^h \leqslant 1$	G	–	4.14	12,569
	UV	4.190	0.18	12,569
	PAR	49.24	2.18	12,569
	NIR	46.65	1.97	12,569

Values observed in Botucatu between 2001 and 2005.

Table 2
Statistical properties of daily values of G, UV, PAR and NIR considering the four sky conditions in terms of daily values of clearness index

Clearness index interval	Radiation component	Fraction of G (%)	Mean (MJ m^{-2})	Standard deviation (%)	Minimum (MJ m^{-2})	Maximum (MJ m^{-2})	Number of days
$K_T^d \leqslant 0.35$	G	–	8.06	40.98	1.05	14.73	217
	UV	4.86	0.39	39.41	0.06	0.72	217
	PAR	51.48	4.15	39.80	0.63	7.42	217
	NIR	43.66	3.52	42.97	0.35	6.69	217
$0.35 < K_T^d \leqslant 0.55$	G	–	16.37	24.33	1.10	33.08	315
	UV	4.41	0.72	25.49	0.04	1.39	315
	PAR	49.57	8.11	24.75	0.52	16.00	315
	NIR	46.02	7.53	23.97	0.54	15.69	315
$0.55 < K_T^d \leqslant 0.65$	G	–	20.34	22.19	12.53	41.90	337
	UV	4.12	0.84	25.38	0.48	1.46	337
	PAR	48.90	9.95	23.04	6.03	19.78	337
	NIR	46.98	9.56	21.31	5.87	20.65	337
$K_T^d > 0.65$	G	–	21.14	23.03	10.11	32.49	490
	UV	3.95	0.84	26.87	0.12	1.29	490
	PAR	48.49	10.25	23.84	5.04	15.73	490
	NIR	47.56	10.05	22.14	4.69	15.55	490
$0 \leqslant K_T^d \leqslant 1$	G	–	17.70	35.69	1.05	41.90	1359
	UV	4.17	0.74	34.70	0.04	1.29	1359
	PAR	49.06	8.68	35.29	0.52	19.78	1359
	NIR	46.77	8.28	36.52	0.35	20.65	1359

Values observed in Botucatu between 2001 and 2005.

fraction (NIR/G) decreases with sky conditions changing from clear to overcast.

The maximum hourly values of G, UV, PAR and NIR can be interpreted as the amplitude of the diurnal evolution and they increase as the cloudy cover decreases (Table 1).

The statistical properties of hourly values of PAR and NIR regardless the sky conditions are similar to the ones observed for sky condition partially cloudy with predominance of diffuse component of the solar radiation (Table 1).

3.3. Daily values

In general, as the cloud cover increases, the UV and PAR fractions of G, based on daily values, increase and the NIR fraction of G decreases (Table 2).

The variation of the daily amplitude, given by the difference between maximum and minimum daily values of UV, PAR and NIR, follows the pattern presented by the hourly values (Section 3.2).

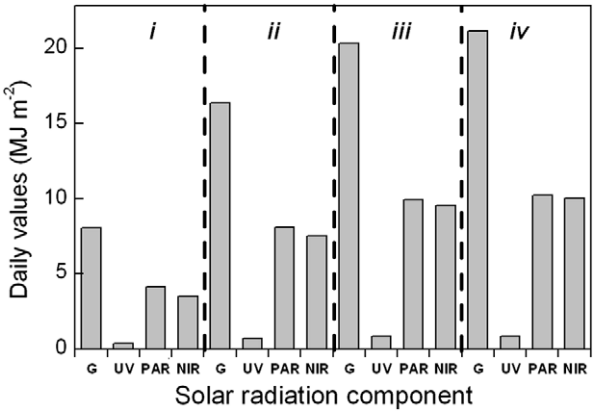

Fig. 4. Daily values of **G**, UV, PAR and NIR observed, at the surface, in Botucatu from 2001 to 2005. Vertical dashed lines define regions of K_T values associated to the sky conditions.

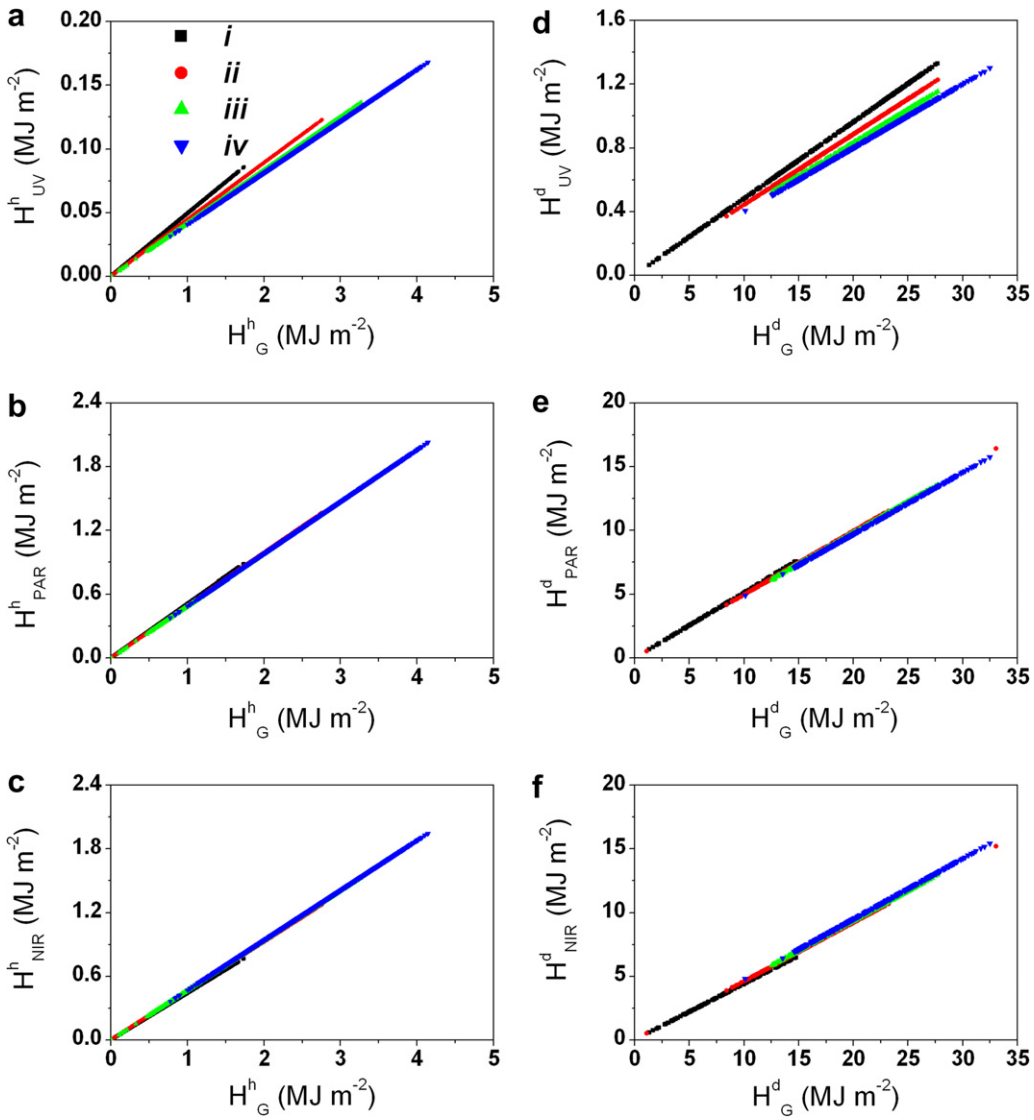

Fig. 5. Dispersion diagram of (a)–(c) hourly and (d)–(f) daily values of UV, PAR and NIR components of solar radiation at the surface in terms of global solar radiation, considering the four categories of clearness index.

Table 3
Expressions to estimate hourly and daily values of UV, PAR and NIR in terms of G and the respective determination coefficient considering the four sky intervals of K_T

Clearness index interval	Hourly values		Daily values	
	Expression	R^2	Expression	R^2
$K_T \leqslant 0.35$	$H^h_{UV} = 0.049H^h_G$	0.9855	$H^d_{UV} = 0.048H^d_G$	0.9699
	$H^h_{PAR} = 0.510H^h_G$	0.9947	$H^d_{PAR} = 0.512H^d_G$	0.9925
	$H^h_{NIR} = 0.041H^h_G$	0.9967	$H^d_{NIR} = 0.440H^d_G$	0.9899
$0.35 < K_T \leqslant 0.55$	$H^h_{UV} = 0.045H^h_G$	0.9622	$H^d_{UV} = 0.0044H^d_G$	0.9622
	$H^h_{PAR} = 0.495H^h_G$	0.9978	$H^d_{PAR} = 0.496H^d_G$	0.9938
	$H^h_{NIR} = 0.461H^h_G$	0.9965	$H^d_{IR} = 0.460H^d_G$	0.9907
$0.55 < K_T \leqslant 0.65$	$H^h_{UV} = 0.042H^h_G$	0.9839	$H^d_{UV} = 0.042H^d_G$	0.9731
	$H^h_{PAR} = 0.490H^h_G$	0.9966	$H^d_{PAR} = 0.490H^d_G$	0.9923
	$H^h_{IR} = 0.469H^h_G$	0.9945	$H^d_{IR} = 0.469H^d_G$	0.9882
$K_T > 0.65$	$H^h_{UV} = 0.041H^h_G$	0.9792	$H^d_{UV} = 0.040H^d_G$	0.9846
	$H^h_{PAR} = 0.489H^h_G$	0.9922	$H^d_{PAR} = 0.485H^d_G$	0.9942
	$H^h_{NIR} = 0.470H^h_G$	0.9894	$H^d_{NIR} = 0.475H^d_G$	0.9931
$0 \leqslant K_T \leqslant 1$	$H^h_{UV} = 0.042H^h_G$	0.9794	$H^d_{UV} = 0.042H^d_G$	0.9204
	$H^h_{PAR} = 0.491H^h_G$	0.9978	$H^d_{PAR} = 0.489H^d_G$	0.9904
	$H^h_{NIR} = 0.468H^h_G$	0.9968	$H^d_{NIR} = 0.469H^d_G$	0.9870

Please cite this article in press as: Escobedo JF et al., Modeling hourly and daily fractions of UV, PAR and NIR to global solar ..., Appl Energ (2008), doi:10.1016/j.apenergy.2008.04.013

Table 4
Hourly values of ultraviolet radiation fraction of global radiation

Location	H^h_{UV}/H^h_G (%)	Land use	Lat, long (°)	Altitude (m)
Valencia (Spain) [17]	2.7 (August) 3.1 (March)	Urban (near to the ocean)	(39°28′N, 00°22′W)	40
Valencia (Spain) [18]	2.9 (January) 3.5 (October)	Urban (near to the ocean)	(39°28′N, 00°22′W)	40
Athalassa (Cyprus) [22]	2.96 (January) 4.12 (September)	Semi-urban	(35°15′N, 33°40′E)	165
Granada (Spain) [14]	3.0 (cloudless sky) 5.0 (cloudy sky)	Rural	(37°10′N, 3°36′E)	660
Potsdam (Germany) [16]	3–4 (typical values) 5–6 (cloudy sky)	Rural	(55°22′N, 13°5′E)	107
Botucatu (Brazil)	**4.0 (clear sky)** **4.9 (cloudy sky)**	**Rural**	(22°53′S, 48°26′W)	**786**
Córdoba (Spain) [12]	3.9(clear sky) 4.5(cloudy sky)	Urban	(37°53′N, 4°46′W)	125
Valencia (Spain) [12]	4.4 (clear sky) 5.6 (cloudy sky)	Urban (near to the ocean)	(39°28′N, 00°22′W)	20
Kwangju (South Korea) [11]	6.9 (November) 8.5 (September)	Urban	(35°10′N, 126°55′E)	90

Table 5
Daily values of ultraviolet radiation fraction of global radiation

Location	H^d_{UV}/H^d_G(%)	Land use	Lat, long (°)	Altitude (m)
Dhahran (Saudi Arabia) [7]	2.1 (dust) 4.5 (rainy)	Desert	(26°16′N, 50°09′E)	–
Valencia (Spain) [17]	2.2 (August) 2.8 (March)	Urban (near to the ocean)	(39°28′N, 00°22′W)	40
Athalassa (Cyprus) [22]	2.59 (January) 3.69 (September)	Semi-urban	(35° 15′N, 33° 40′E)	165
Valencia (Spain) [18]	2.8 (January) 3.4 (October)	Urban (near to the ocean)	(39°28′N, 00°22′W)	40
Makkah (Saudi Arabia) [8]	2.8–4.3	Urban	(21°30′N, 41°0′E)	–
Cairo (Egypt) [9]	3.3–3.4 (dusty)	Urban	(30°05′N, 31°17′E)	–
Bahtim (Egypt) [9]	2.5–3.2 (clear sky)	Rural	(30°08′N, 31°15′E)	–
Botucatu, Brazil	**4.0–4.8**	**Rural**	(22°53′S, 48°26′W)	**786**
Kuwait (Saudi Arabia) [10]	4.2 (December) 5.2 (August)	Urban	(29°22′N, 47°58′E)	–

Table 6
Hourly values of photosynthetically active radiation fraction of global radiation

Location	H^h_{PAR}/H^h_G (%)	Land use	Lat, long (°)	Altitude (m)
Athalassa (Cyprus) [42]	41.1 (clear sky) 44.0 (cloudy sky)	Semi-rural	(35°15′N, 33°40′E)	165
Athens (Greece) [43]	43.4 (clear sky) 44.2 (intermediate sky) 46.1 (cloudy sky)	Urban	(37°58′N, 23°43′E)	205
Guelph, Ontario (Canada) [31]	45.1 (clear sky) 54.0 (cloudy sky)	Rural	43°33′N, 80°15′W)	334
Ilorim (Niger) [37]	45.3 (clear sky) 47.0 (cloudy sky)	Rural	(8°32′N, 4°34′E)	375
Athens (Greece) [34]	48.0 (clear sky) 49.0 (cloudy sky)	Urban	(37°58′N, 23°43′E)	107
Botucatu (Brazil)	**48.9 (clear sky)** **51.0 (cloudy sky)**	**Rural**	**(22°53′S, 48°26′W)**	**786**
Dar es Salaam (Tanzania) [29]	51.0 (clear sky) 63.0 (cloudy sky)	Urban	(6°48′S, 39°17′E)	0

For the standard deviation daily values of G, UV, PAR and NIR the variation in terms of the sky condition oscillated between 20% and 40% (Table 2). Considering all the solar radiation components, the largest standard deviation (about 40%) occurs for cloudy sky ($K_T \leqslant 0.35$). Sky conditions with $K_T > 0.35$ present standard deviations varying between 21% and 27% (Table 2).

Please cite this article in press as: Escobedo JF et al., Modeling hourly and daily fractions of UV, PAR and NIR to global solar ..., Appl Energ (2008), doi:10.1016/j.apenergy.2008.04.013

Table 7
Daily values of photosynthetically active radiation fraction of global radiation

Location	H^d_{PAR}/H^d_G (%)	Land use	Lat, long (°)	Altitude (m)
Athalassa (Cyprus) [42]	40.8 (clear sky) 42.1 (intermediate sky) 44.0 (overcast)	Semi-rural	(35°15′N, 33°40′E)	165
Lusaka (Zâmbia) [41]	41.9 (clear sky) 46.2 (cloudy sky)	Biomass burning	(15°24′S, 28°18′E)	1154
Llorim (Niger) [37]	44.2 (dry weather) 46.4 (wet weather)	Rural	(8°32′N, 04°34′E)	375
Corvallis, Oregon (USA) [33]	44.3 (clear sky) 44.7 (partially cloudy sky) 48.3 (cloudy sky)	Semi-urban	(44°34′N, 123°14′W)	65.5
Athens (Greece) [34]	46.8 (clear sky) 47.2 (cloudy sky)	Urban	(37°58′N, 23°43′E)	107
Botucatu (Brazil)	48.5 (clear sky) 51.2 (cloudy sky)	**Rural**	**(22°53′S, 48°26′W)**	**786**

In the case of the amplitude – difference between maximum and minimum daily values – the variation in terms of the sky conditions is controlled basically by astronomical effects (Table 2). In the case of Botucatu, the amplitude of all four solar radiation components for clear sky condition is larger than for cloudy condition. However, the largest frequency of clear skies occurs during winter period, when the amplitude of G is smaller, Botucatu has a large frequency of clear sky conditions also during summer [53,60].

The statistical properties of daily values of G, UV, PAR and NIR regardless the sky conditions are close to the ones observed for sky condition partially cloudy with predominance of diffuse component of the solar radiation (Table 2).

Fig. 4 shows the daily values of G, UV, PAR and NIR averaged in terms of the sky condition. The largest difference occurs between sky conditions *i* (cloudy) and *ii* (partially cloudy with predominance of diffuse component of solar radiation). In this case, daily values of G, UV, PAR and NIR varied around 100%. The smallest difference occurs between conditions *iii* (partially cloudy with pre-

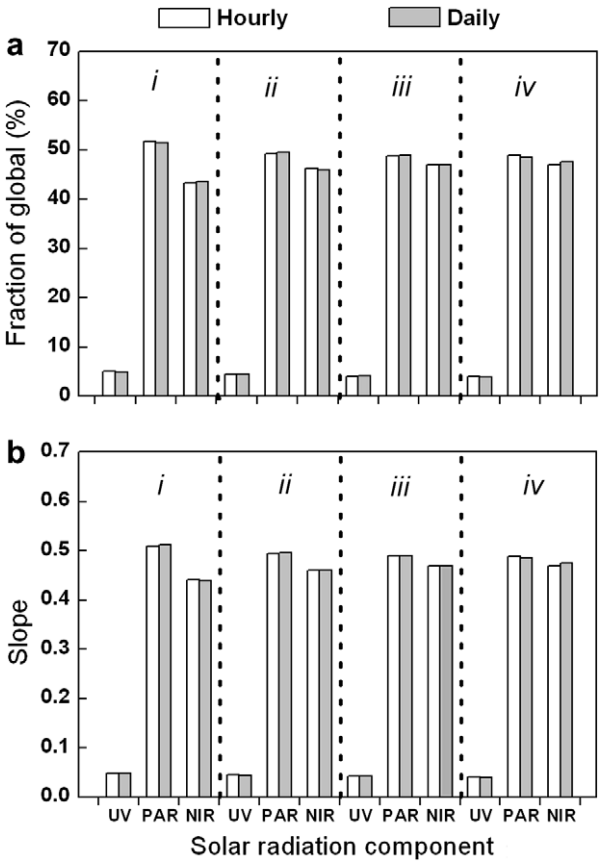

Fig. 6. (a) Fraction of global solar radiation represented by UV, PAR and NIR components and (b) slope of the best-fit straight line interpolated linear regression passing by the origin. Hourly and daily values observed in Botucatu considering the four sky conditions.

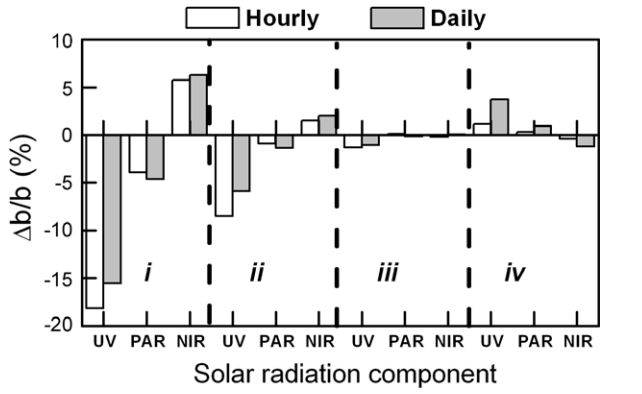

Fig. 7. Comparison between the slope obtained from observed values of UV, PAR and NIR components considering the 4 sky condition categories (b_{sky}) and without sky condition consideration ($b_{without}$). $\Delta b/b = 100\%\ (b_{sky} - b_{without})/b_{without}$.

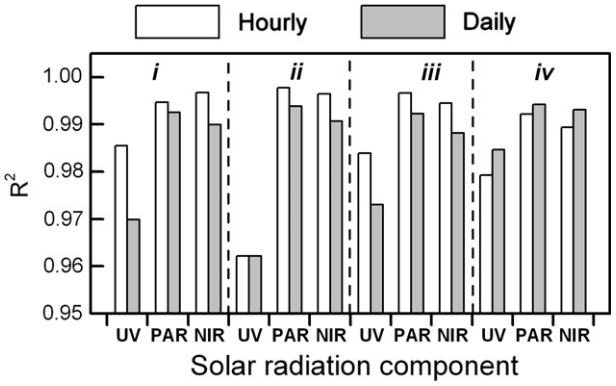

Fig. 8. Coefficient of determination (R^2) of modeled values of UV, PAR and NIR components considering the 4 sky conditions. Hourly and daily values observed in Botucatu during 2005.

dominance of direct component of solar radiation) and *iv* (clear sky), varying from 0% (UV) to about 5% (NIR).

3.4. Linear regression modeling

Fig. 5 indicates the correlation between the solar component radiations and G for hourly and daily values, considering sky conditions defined by the four clearness index intervals described in Section 4. Table 3 shows the linear expressions and their respective determination coefficients for hourly and daily values. For reference, it was included in Table 3 the linear expressions and determination coefficients for hourly and daily values estimated not considering sky conditions. These expressions are valid for Botucatu for $0 \leqslant K_T \leqslant 1$.

The slope of the best-fit straight line interpolated by linear regression varied as a function of the sky cover. The slopes b^h_{UV} and b^h_{PAR} decrease with K_T, while b^h_{NIR} increases with K_T. Similar behavior is observed for daily values (Table 3).

The slopes b^h_{UV} (=0.049), b^d_{UV} (=0.048), b^h_{PAR} (=0.510) and b^d_{PAR} (=0.512) are larger in the interval $K_T \leqslant 0.35$ and they decrease as K_T increases. By the other hand, the slopes b^h_{NIR} (=0.441) and b^d_{NIR} (=0.440) are smaller in the interval $K_T \leqslant 0.35$ and they increase as K_T increases.

Considering that b_{UV} is an indicative of the G fraction represented by the UV component, the linear regression indicates that for hourly values H^h_{UV} under cloudy sky and clear sky represent, respectively, 4.9% and 4.1% of G in Botucatu. These values are in agreement with the literature (Table 4). Similarly, daily values of H^d_{UV} under cloudy sky and clear sky conditions represent, respectively 4.8% and 4.0% of G in Botucatu. Theses values are higher than the values found in most of the literature (Table 5).

Table 8
Means bias error (MBE), root mean square error (RMSE) and index of agreement (*d*) estimated from empirical expressions of hourly and daily values of UV, PAR and NIR in terms of G considering the four sky intervals of K_T. Values observed in Botucatu during 2005

Clearness index interval	Radiation component	Hourly values			Daily values		
		MBE (%)	RMSE (%)	*d*	MBE (%)	RMSE (%)	*d*
$K_T \leqslant 0.35$	UV	−3.18	10.36	0.9942	−1.89	7.36	0.9897
	PAR	−1.72	5.21	0.9986	−1.62	2.95	0.9985
	NIR	2.45	7.15	0.9975	1.93	3.68	0.9979
$0.35 < K_T \leqslant 0.55$	UV	0.15	8.22	0.9916	−4.80	6.82	0.9929
	PAR	−0.36	3.30	0.9986	−1.19	2.27	0.9993
	NIR	0.38	4.09	0.9977	1.80	3.00	0.9989
$0.55 < K_T \leqslant 0.65$	UV	1.15	8.74	0.9848	−2.12	6.87	0.9872
	PAR	−0.23	3.35	0.9974	0.05	2.20	0.9989
	NIR	0.14	4.02	0.9958	0.13	2.68	0.9985
$K_T > 0.65$	UV	0.95	6.27	0.9878	0.09	4.03	0.9942
	PAR	−0.08	3.97	0.9944	0.20	2.01	0.9986
	NIR	0.00	4.38	0.9925	−0.21	2.20	0.9985

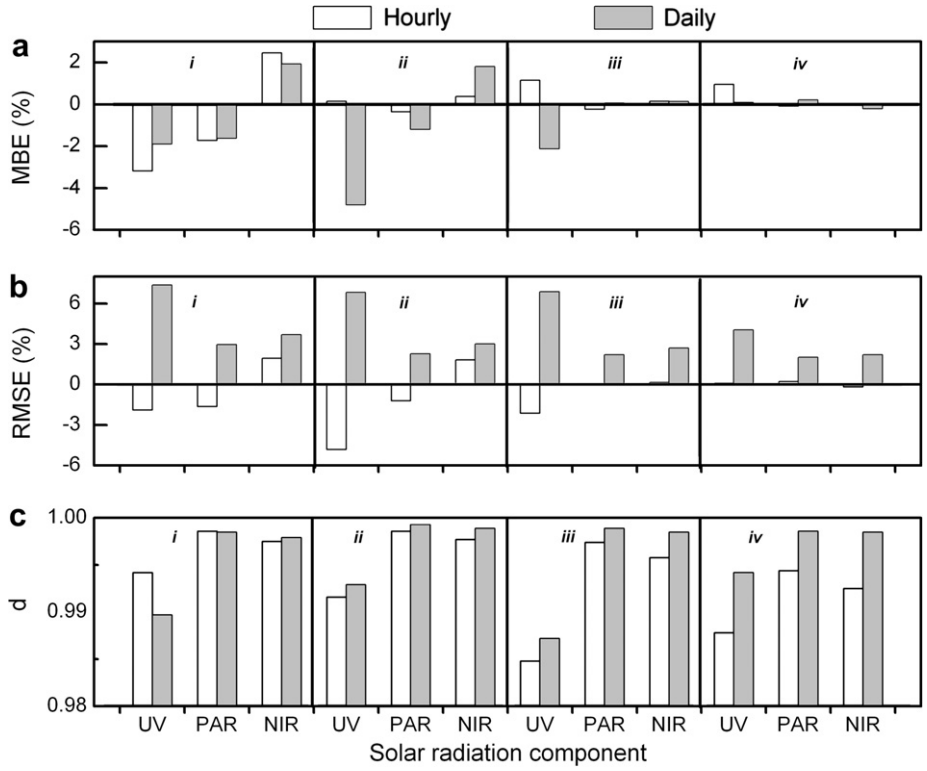

Fig. 9. (a) MBE, (b) RMSE and (c) index of agreement as a function of the sky conditions for hourly and daily values of solar radiation.

In the case of the b_{PAR}, for Botucatu, the linear regression indicates that under cloudy sky and clear sky the hourly values of H^h_{PAR} represent, respectively, 51% and 48.9% of H^d_G and the daily values of H^d_{PAR} represent, respectively, 51.2% and 48.5% of H^d_G. The Botucatu values are higher than the values found in most of the literature (Tables 6 and 7).

Fig. 6 shows the matching between the fraction (Fig. 6a) and the slope (Fig. 6b) in the case of hourly and daily values, considering the four intervals of sky conditions.

Comparing the slopes for hourly and daily values considering sky conditions (Fig. 7 and Table 3) and regardless sky conditions (Tables 4 and 6), it is possible to infer that the best agreement is between the expression for cloudy sky condition *iii* ($0.55 < K_T \leqslant 0.65$). This result confirmed the predominance of cloudy sky condition *iii* on the local climate of Botucatu indicated by the similarity of the statistical properties of G, UV, PAR and NIR (Sections 3.2 and 3.3).

According to Fig. 7, the largest discrepancy is observed for the hourly UV component in cloudy sky condition (condition *i*). In this case, the UV radiation difference is 18% (Fig. 7).

The model developed without considering sky conditions perform better for PAR and NIR with the difference within |8%|.

The coefficient of determination (R^2) for the hourly (daily) value expressions of UV, PAR and NIR components in terms of hourly (daily) values of G are indicated in Table 3 and Fig. 8. Similarly, to the hourly values, the expressions for PAR show the largest coefficient of determination and for UV the smallest. Usually they are equal or greater than 0.96 for hourly and daily values. The model performed better for clear sky conditions (Fig. 8).

The R^2 obtained for UV component in function of G are of the same order of those obtained by Martinez-Lozano and Casanovas [17], Martinez-Lozano et al. [18], Cañada et al. [12], Ogunjobi and Kim [11] and Jacovides et al. [22].

For PAR component, the R^2 values obtained for Botucatu were also similar to the literature [27,30–31,34–36,39,43].

3.5. Validation results

The accuracy of the model's predictions is evaluated through mean bias error (MBE) and root mean square error (RMSE). These statistical indicators are given here as the percentage of the respective mean measured radiant flux component.

The MBE, RMSE and d for the hourly and daily values of UV, PAR and NIR component radiations are indicated in Table 8 and Fig. 9.

In general, the MBE for hourly and daily values were situated between ±5.0% interval, indicating a good performance of hourly and daily models for UV, PAR and NIR. The values of RMSE for hourly and daily values were below 10.4%.

The best performances were obtained using the expressions for daily values of PAR, with RMSE varying from 2.01% for clear sky ($K^d_T > 0.65$) to 2.95% for cloudy condition ($K^d_T \leqslant 0.35$) and for hourly values of PAR, with 3.3% for partially cloudy with predominance of diffuse solar radiation ($0.35 < K^h_T \leqslant 0.55$) to 5.21% for cloudy condition ($K^h_T \leqslant 0.35$).

The modeled daily values of NIR presented values of RMSE varying from 2.2% under clear sky conditions to 3.68% under cloudy conditions. The RMSE for hourly values of NIR varied from 4.02% for partially cloudy with predominance of direct component of the solar radiation to 7.15% for cloudy conditions.

The largest values of RMSE were obtained for the modeled daily and hourly values of UV.

The index of agreement were systematically superior to 0.98 (Fig. 9c) indicating the good agreement between modeled and observed daily and hourly values of UV, PAR and NIR.

In general, the indexes of agreement for daily values were larger than for hourly values. The hourly values performed better than daily values only under cloudy conditions. The PAR showed slightly larger indexes of agreement for hourly and daily values than the NIR and UV components in the four sky conditions intervals.

4. Conclusions

In this work, expressions to predict daily and hourly values of UV, PAR and NIR components of solar radiation at the surface in terms of global solar radiation also measured at the surface were developed for four classes of sky conditions defined objectively in terms of the clearness index.

The sky condition classes were developed using hourly values of global, diffuse and direct solar radiation, at the surface, block-averaged in terms of clearness index (K_T). It was considered continuous measurement of these parameters in Botucatu between 1995 and 2003.

Hourly and daily values of UV, PAR and NIR are linearly correlated with hourly and daily values of global solar radiation measured at the surface using observations carried out between 2001 and 2004. A set of linear regression expressions, with zero intercept, were derived in terms of four classes of sky conditions.

The set of equations derived for Botucatu indicate that sky conditions, cloudy cover, it is only important for UV component. PAR and NIR components of solar radiation at the surface are less dependent of the cloudy cover.

Using hourly and daily values observed in 2005, the linear regression model performances were analyzed in terms of determination coefficient. In general, all linear regression expressions performed well, with R^2 close to 1. Expressions for hourly values performed better than for daily values of UV, PAR and NIR.

The slopes of the best-fit straight line interpolated by linear regression – equivalent to the global fraction of UV, PAR and NIR – varied as a function of K_T for hourly and daily values.

The validation tests, carried out in terms of index of agreement, *MBE* and *RMSE* indicated that the linear regression models have a good performance for both hourly and daily values.

The expressions obtained for condition *iii* (partially cloudy with predominance of direct component of the solar radiation) match the expressions proposed for all sky conditions. The linear regression models derived to estimate PAR and NIR components may be obtained without sky condition considerations, within a maximum variation of 8%. However, in the case of UV, not taking into consideration the sky condition may cause a discrepancy of up to 18% for hourly values and 15% for daily values.

Considering the sky condition is important for developing linear regression models to estimate UV radiation in terms of G because in the presence of clouds the associated high content of water vapour in the atmosphere alters G more than UV. How the other minor atmospheric constituents, such as aerosol and ozone affect UV, PAR and NIR components at the surface will be investigated in future work.

References

[1] Jiménez AE, Estrada CA, Cota AD, Román A. Photocatalytic degradation of DBSNa using solar energy. Sol Energy Mater Sol Cells 2000;60:85–95.
[2] Kelly CT, White JR. Photo-degradation of polyethylene and polypropylene at slow strain-rate. Polym Degrad Stabil 1997;56:367–83.
[3] Parisi AV, Wong JCF. An estimation of biological hazards due to solar radiation. J Photochem Photobiol B: Biol 2000;54:126–30.
[4] Jacob . Heterogeneous chemistry and tropospheric ozone . Atmos Environ 2000;34:2131–59.
[5] Dodge MC. Chemical oxidant mechanisms for air quality modeling: critical review. Atmos Environ 2000;34:2103–30.
[6] Rao CRN, Takoshima T, Bradley WA, Lee TY. Near ultraviolet radiation at the earths surface: measurements and model comparison. Tellus 1984;36B:286–93.
[7] Elhadidy MA, Abdel-Nabi DY, Kruss PD. Ultraviolet solar radiation at Dhahram (Saudi Arabia). Solar Energy 1990;44:315–9.

Please cite this article in press as: Escobedo JF et al., Modeling hourly and daily fractions of UV, PAR and NIR to global solar ..., Appl Energ (2008), doi:10.1016/j.apenergy.2008.04.013

[8] Khogali A, Al-Bar OF. A study of solar ultraviolet radiation at Makkah solar station. Solar Energy 1992;48:79–87.
[9] Robaa SM. A study of ultraviolet solar radiation at Cairo urban area, Egypt. Solar Energy 2004;77:251–9.
[10] Al-Aruri SD, Rasas M, Al-Jamal K, Shaban N. An assessment of global UV solar radiation in the range (0.290–0.385 μm) in Kuwait. Solar Energy 1988;41:159–62.
[11] Ogunjobi KO, Kim YJ. Ultraviolet (0.280–0.400 (m) and broadband solar hourly radiation at Kwangju, South Korea: analysis of their correlation with aerosol optical depth and clearness index. Atmos Res 2004;71:193–214.
[12] Cañada J, Pedrós G, Bosca JV. Relationship between UV (0.290–0.385 μm) and broad band solar radiation hourly values in Valencia and Córdoba, Spain. Energy 2003;28:199–217.
[13] Foyo-Moreno I, Vida J, Alados-Arboledas L. A simple all weather model to estimate ultraviolet solar radiation (290–385 nm). J Appl Meteorol 1998;38:1020–6.
[14] Foyo-Moreno I, Vida J, Alados-Arboledas L. Ground based ultraviolet (290–385 nm) and broadband solar radiation measurements in south-eastern Spain. Int J Climatol 1998;18:1389–400.
[15] Al-Aruri SD. The empirical relationship between global radiation and global ultraviolet (0.290–0.385) μm solar radiation component. Solar Energy 1990;45:61–4.
[16] Feister U, Grasnick K-H. Solar UV radiation measurements at Potsdam 5'E)(55°22′N, 13°5′E). Solar Energy 1992;49:541–8.
[17] Martinez-Lozano JA, Casanovas AJ. Comparison of global ultraviolet (290–385 nm) and global irradiation measured during the warm season in Valencia, Spain. Int J Climatol 1994;14:93–102.
[18] Martinez-Lozano JA, Tena F, Utrillas MP. Ratio of UV to global broad band irradiation in Valencia, Spain. Int J Climatol 1999;19:903–11.
[19] Cañada J, Pedrós G, López A, Bosca JV. Influences of the clearness index in the whole spectrum and of the relative optical air mass on UV solar irradiance for two locations in the Mediterranean area, Valencia and Córdoba. J Geophys Res 2000;105:4759–66.
[20] Foyo-Moreno I, Alados I, Olmo FJ, Alados-Arboledas L. The influence of cloudiness on UV global irradiance (295–385 nm). Agr Forest Meteorol 2003;120:101–11.
[21] Murillo W, Cañada J, Pedrós G. Correlation between global ultraviolet (290–385 nm) and global irradiation in Valencia and Cordoba (Spain). Renew Energy 2003;28:409–18.
[22] Jacovides CP, Assimakopoulos VD, Tymvios FS, Theophilou K, Asimakopoulos DN. Solar global UV (280–380 nm) radiation and its relationship with solar global radiation measured on the island of Cyprus. Energy 2006;31:2728–38.
[23] Ackerly DD, Bazzaz FA. Seedling crown orientation and interception of diffuse radiation in tropical forest gaps. Ecology 1995;76:1134–46.
[24] Cannel MGR, Grace J. Competition for light: detection, measurement and quantification. Can J Forest Res 1993;23:1969–79.
[25] Baldocchi D, Hutchinson B, Matt D, Mcmitten R. Seasonal variations in the radiation regime within oakhickory forest. Agr Forest Meteorol 1984;33:177–91.
[26] Szeicz G. Solar radiation for plant growth. J Appl Ecol 1974;11:617–36.
[27] Britton CM, Dodd JD. Relationships of photosynthetically active radiation and shortwave irradiance. Agr Meteorol 1976;17:1–7.
[28] Stanhill G, Fuchs M. The relative flux density of photosynthetically active radiation. J Appl Ecol 1977;14:317–22.
[29] Stigter CJ, Musabilha MM. The conservative ratio of photosynthetically active to total radiation in the tropics. J Appl Ecol 1982;19:853–8.
[30] Howell TA, Meek DW, Hatfield JL. Relationship of photosynthetically active radiation to shortwave radiation in the San Joaquin Valley. Agr Meteorol 1983;28:157–75.
[31] Blackburn WJ, Proctor JTA. Estimating photosynthetically active radiation from measured solar irradiance. Solar Energy 1983;31:233–4.
[32] McCree KJ. Daily photosynthesis totals calculated from solar radiation histograms. Agr Forest Meteorol 1984;33:239–48.
[33] Rao CRN. Photosynthetically active components of global solar radiation: measurements and model computations. Arch Meteorol Geophys Bioclimatol 1984;34:353–64.
[34] Papaioannou G, Papanikolaou N, Retalis D. Relationships of photosynthetically active radiation and shortwave irradiance. Theor Appl Climatol 1993;48:23–7.
[35] Papaioannou G, Nikolidakis G, Asimakopoulus DN, Retalis D. Photosynthetically active radiation in Athens. Agr Forest Meteorol 1996;81: 287–98.
[36] Alados I, Foyo-Moreno I, Alados-Arboledas L. Photosynthetically active radiation: measurements and modelling. Agr Forest Meteorol 1996;78:121–31.
[37] Udo SO, Aro TO. Global PAR related to solar radiation for central Nigeria. Agr Forest Meteorol 1999;97:21–31.
[38] Alados I, Olmo FJ, Foyo-Moreno I, Alados–Arboledas L. Estimation of photosynthetically active radiation under cloudy conditions. Agr Forest Meteorol 2000;102:39–50.
[39] Alados-Arboledas L, Olmo FJ, Alados I, Pérez M. Parametrics models to estimate photosynthetically active radiation in Spain. Agr Forest Meteorol 2000;101:187–201.
[40] Tsubo M, Walker S. Relationships between photosynthetically active radiation and clearness index at Bloemfontein, South Africa. Theor Appl Climatol 2005;80:17–25.
[41] Finch DA, Bailey WG, Mcarthur LJB, Nasitwitwi M. Photosynthetically active radiation regimes in a southern African savanna environment. Agr Forest Meteorol 2004;122:229–38.
[42] Jacovides CP, Timvios FS, Papaioannou G, Asimakopoulos DN, Theofilou CM. Ratio of PAR to broadband solar radiation measured in Cyprus. Agr Forest Meteorol 2004;121:135–40.
[43] Jacovides CP, Tymvios FS, Assimakopoulos VD, Kaltsounides NA. The dependence of global and diffuse PAR radiation components on sky conditions at Athens, Greece. Agr Forest Meteorol 2007;143:277–87.
[44] Jacovides CP, Timbios F, Asimakopoulos DN, Steven MD. Urban aerosol and clear skies spectra for global and diffuse photosynthetically active radiation. Agr Forest Meteorol 1997;87:91–104.
[45] Larsen N F, Stamnes K. Use of shadows to retrieve water vapor in hazy atmospheres. Appl Optics 2005;44:6986–94.
[46] Pereira AR, Machado EC, de Camargo MBP. Solar radiation regime in three cassava (Manihot sculenta Grantz) canopies. Agr Meteorol 1982;26:1–10.
[47] Zhang X, Zhang Y, Zhoub Y. Measuring and modelling photosynthetically active radiation in Tibet Plateau during April–October. Agr Meteorol 2000;102:207–12.
[48] Bolsenga SJ. Near Infrared Radiation in Northern Greenland. J Appl Meteorol 1967;6:449–51.
[49] Yang X, Miller DR. Calculation of potential broadband biological active and thermal solar radiation above vegetation canopies. J Appl Meteorol 1995;34:861–72.
[50] Spinoza RC, Harshvardhan. Parameterization of solar near-infrared radiative properties of cloudy layers. J Appl Meteorol 1996;53:1559–68.
[51] Iqbal M. An introduction to solar radiation. New York: Academic Press; 1983. pp. 390.
[52] Pérez R, Ineichen P, Seals R, Michalsky JJ, Stewart R. Modelling daylight availability and irradiance components from direct and global irradiance. Solar Energy 1990;44:271–89.
[53] Assunção FH, Escobedo JF, Oliveira AP. A new algorithm to estimate sky condition based on 5 min-averaged values of clearness index and relative optical air mass. Theor Appl Climatol 2007;90:235–48.
[54] Fröhlich C, London J. Revised Instruction manual on radiation instruments and measurements. WCRP Publications series No. 7. WMO/TD No. 149, October 1986.
[55] Mccree KJ. Test of current definitions of photosynthetically active radiation against leaf photosynthesis data. Agr Meteorol 1972;10:443–53.
[56] Frölich C, Lean J. The sun's total irradiance: Cycles and trends in the past two decades and associated climate change uncertainties. Geophys Res Lett 1998;25:4377–80.
[57] Oliveira AP, Escobedo JF, Machado AJ, Soares J. Diurnal evolution of solar radiation at the surface in the City of São Paulo: seasonal variation and modeling. Theor Appl Climatol 2002;71:231–49.
[58] Oliveira AP, Escobedo JF, Machado AJ, Soares J. Correlation models of diffuse solar radiation applied to the City of São Paulo (Brazil). Appl Energy 2002;71(1):59–73.
[59] Soares J, Oliveira AP, Boznar MZ, Mlakar P, Escobedo JF, Machado AJ. Modeling hourly diffuse solar radiation in the city of São Paulo using neural network technique. Appl Energy 2004;79:201–14.
[60] Assunção FH, Escobedo JF, Oliveira AP. Modelling frequency distributions of 5 min-averaged solar radiation indexes using Beta probability functions. Theor Appl Climatol 2003;75:213–24.

Please cite this article in press as: Escobedo JF et al., Modeling hourly and daily fractions of UV, PAR and NIR to global solar ..., Appl Energ (2008), doi:10.1016/j.apenergy.2008.04.013